The Journal of CPRI,
Vol. 10, No. 4, December 2014 pp. 785-798

Steady State and transient performance of an inverter based microgrid

Jyothsna T R*, Ramya Sree B*, Ramya V*, Deshpande R A**

The analysis of small-signal stability of conventional power systems is well established, but for inverter based microgrids there is a need to establish how circuit and control features gave rise to particular oscillatory modes and which of these have poor damping. This paper develops the modeling and stability analysis of autonomous operation of inverter based microgrids. Each sub-module is modeled in state-space form and all are combined together on a common reference frame. The model captures the detail of the control loops of the inverter but not the switching action. Some inverter modes are found at relatively high frequency and so a full dynamic model of the network (rather than an algebraic impedance model) is used. The complete models linearized around an operating point and the resulting system matrix is used to derive the eigenvalues. The eigenvalues (termed "modes") indicate the frequency and damping of oscillatory components in the transient response. A sensitivity analysis is also presented which helps identifying the origin of each of the modes and identifies possible feedback signals for design of controllers to improve the system stability. With experience it is possible to simplify the model (reduce the order) if particular modes are not of interest as is the case with synchronous machine models. Transient stability results have been obtained from a microgrid of three 10-kVA inverters.

Keywords: *Inverter, inverter model, microgrid, power control, small-signal stability, transient Stability*

1.0 INTRODUCTION

Recent innovations in small-scale distributed power generation systems combined with technological advancements in power electronic systems led to concepts of future network technologies such as microgrids. These small autonomous regions of power systems can offer increased reliability and efficiency and can help integrate renewable energy and other forms of distributed generation (DG) [1]. Many forms of distributed generation such as fuel-cells, photo-voltaic and micro-turbines are interfaced to the network through power electronic converters [2]–[5]. These interface devices make the sources more flexible in their operation and control compared to the conventional electrical machines. However, due to their negligible physical inertia they also make the system potentially susceptible to oscillation resulting from network disturbances.

A microgrid can be operated either in grid connected mode or in stand-alone mode. In grid connected mode, most of the system-level dynamics are dictated by the main grid due to the relatively small size of micro sources. In stand-alone mode, the system dynamics are dictated by micro sources themselves, their power regulation control and, to an unusual degree, by the network itself.

*Department of Electrical Engineering, AU College of Engineering, Andhra University,Visakhapatnam
**Central Power Research Institute, Bangalore.

One of the important concerns in the reliable operation of a microgrid is small-signal stability. In conventional power systems, stability analysis is well established and for the different frequency ranges (or time horizons) of possible concern there are models which include the appropriate features. The features have been established on the basis of decades of experience so that there are standard models of synchronous machines, governors and excitation systems of varying orders that are known to capture the important modes for particular classes of problem. This does not yet exist for microgrids and may be difficult to achieve because of the range of power technologies that might be deployed. However, we can begin by developing full-order models of inverters and the inverter equivalents of governors and exciters. Examination of these models applied to various systems will develop that body of experience that allows reduced order models to be selected for some problems.

In this paper, a systematic approach to modeling an inverter-based microgrid is presented [6-18]. Each DG inverter will have an outer power loop based on droop control to share the fundamental real and reactive powers with other DGs. Inverter internal controls will include voltage and current controllers which are designed to reject high frequency disturbances and damp the output LC filter to avoid any resonance with the external network. The small-signal state-space model of an individual inverter is constructed by including the controllers, output filter and coupling inductor on a synchronous reference frame whose rotation frequency is set by the power controller of that inverter. An arbitrary choice is made to select one inverter frame as the common reference frame and all other inverters are translated to this common reference frame using the simple transformation techniques familiar in synchronous machine systems. It is considered that state-less impedance models of the network are inadequate for use with full-order inverter models which include high frequency modes. Instead a dynamic (state-space) model of the network is formed on the common reference frame.

Once the small-signal model has been formed, eigenvalues (or modes) are identified that indicate the frequency and damping of the oscillatory terms of the system transient response. The analytical nature of this examination then allows further investigation so that the relation between system stability and system parameters, such as the gains of controllers is established. A sensitivity analysis is then conducted which provides the sensitivity of different modes to the system state variables and points out the role of each controller in forming of these modes. States associated with modes that are not of interest in a particular problem can then be considered for removal from the model in order to simplify the analysis. This represents a systematic approach to finding appropriate models and avoids the danger of neglecting a system feature that later turns out to be important.

2.0 MICROGRID MODEL IN AUTONOMOUS OPERATION

The modeling approach presented in this paper divides the whole system into three major sub-modules; inverter, network and loads (Figure 1). Each inverter is modeled on its individual reference frame whose rotation frequency is set by its local power sharing controller. The inverter model includes the power sharing control dynamics, output filter dynamics, coupling inductor dynamics and voltage and current controller dynamics. These last two elements introduce high frequency dynamics which are apparent at peak and light load conditions and during large changes in load.

Network dynamics are generally neglected in small-signal modeling of conventional power systems. The reason behind this is that the time constants of rotating machines and their controls are much larger than those of the network. In the case of microgrids, the micro sources are connected through inverters whose response times are very small and network dynamics would influence the system stability. Previous work [6] on small-signal modeling on parallel connected inverters was carried out without considering the network dynamics. Here, the state equations of the network and the loads are represented on the reference frame of one of the individual inverters.

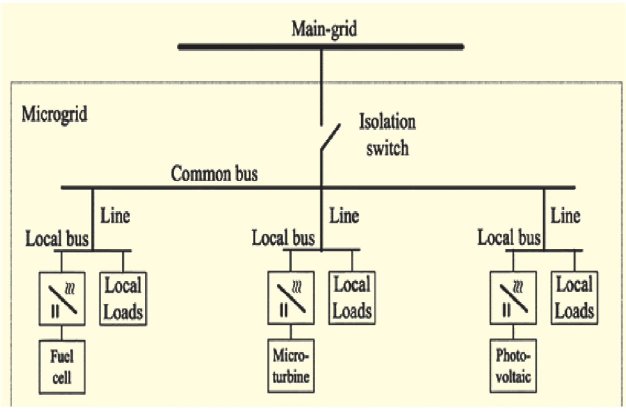

FIG. 1 BLOCK DIAGRAM OF COMPLETE SMALL SIGNAL STATE-SPACE MODEL OF MICROGRID

This reference frame is considered as the common reference frame. All the other inverters are translated to this common reference frame using the transformation technique [11]. Here, the axis set (D-Q) is the common reference frame *ωcom* rotating at a frequency, whereas axes *(d-q)* i and *(d-q) j* are the reference frame of i^{th} the and j^{th} inverters rotating at and , respectively. δ_i is the angle of the reference frame of the i^{th} inverter with respect to the common reference frame. In the following sections the internal modeling of all the three modules is discussed in more detail. It is to be noted that in the equations of the following sections the three phase voltages and currents are represented as vectors in reference frame, where as the other variables such as real and reactive powers and angles are scalars.

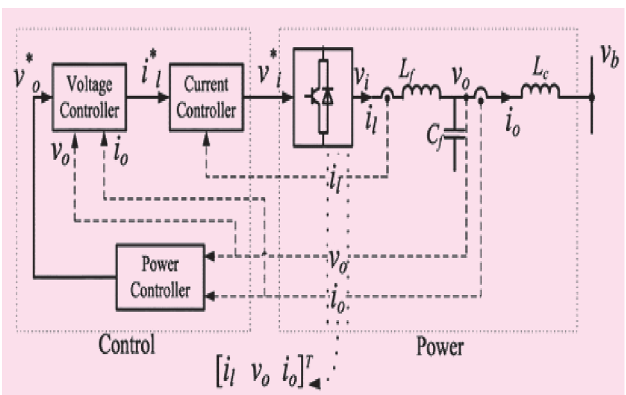

FIG. 2 DG INVERTER BLOCK DIAGRAM

2.1 State-Space Model of A Voltage Source Inverter

Voltage source inverter is commonly used to interface distributed generators to the network. Figure 2 shows the block diagram of an inverter connected to the microgrid. The power processing section consists of a three-leg inverter, an output LC filter and coupling inductor. Assuming an ideal source from the side, DG the dc bus dynamics can be neglected. With the realization of high switching frequencies (4–10 kHz), the switching process of the inverter may also be neglected.

The controller of a DG inverter can be divided into three different parts. First is an external power control loop which sets the magnitude and frequency (and hence phase) for the fundamental component of the inverter output voltage according to the droop characteristics set for the real and reactive powers (harmonic power sharing has been treated as an additional function with a different control topology [12]). The second and third parts of the control system are the voltage and current controllers, which are designed to reject high frequency disturbances and provide sufficient damping for the output LC filter [12], [13]. In this section, a state space model is presented for all of the subsystems: control loops, output filter and coupling inductor. The models are constructed in a rotational reference frame set by the external power controller of the particular individual inverter.

2.2 Power Controller

The basic idea behind the droop control is to mimic the governor of a synchronous generator. In a conventional power system, synchronous generators will share any increase in the load by decreasing the frequency according to their governor droop characteristic. This principle is implemented in inverters by decreasing the reference frequency when there is an increase in the load. Similarly, reactive power is shared by introducing a droop characteristic in the voltage magnitude.

The instantaneous active and reactive power components $\tilde{p}$ and $\tilde{q}$ are calculated from the measured output voltage and output current as in

$$\tilde{p} = v_{od}i_{od}+v_{oq}i_{oq}\tilde{q}=v_{od}i_{oq} - v_{oq}i_{od} \quad ....(1)$$

The instantaneous power components are passed through low-pass filters, shown in (1), to obtain the real and reactive powers *P* and *Q* corresponding to the fundamental component. ω_c represents the cut-off frequency of low-pass filters

$$P = \frac{\omega_c}{s+\omega_c}\tilde{p},\ Q = \frac{\omega_c}{s+\omega_c}\tilde{q} \quad ...(2)$$

The real power sharing between inverters is obtained by introducing an artificial droop in the inverter frequency as in (2). The frequency ω is set according to the droop gain (mp) and phases set by integrating the frequency. This mimics to governor and inertia characteristics of conventional generators and provides a degree of negative feedback. For instance, if the power drawn from a generator increases then the rotation of its voltage slows and its angle retards. In the following equations ω_n will represent the nominal frequency set-point whereas α is the angle of the inverter reference frame seen from a reference frame rotating at (ω_n). From (3) it can be seen that the angle of the inverter voltage, α, changes in response to the real power flow in the required negative sense and with a gain set by the droop

$$\omega = \omega_n - m_p P, \dot{\theta} = \omega, \theta = \omega_n t - \int m_p P dt$$

$$\propto = -\int m_p.Pdt\,, \dot{\propto} = -m_p P \quad ...(3)$$

To share the reactive power among multiple inverters, a droop is introduced in the voltage magnitude as given in (4). Here, V_n stands for the nominal set point of *d*-axis output voltage. The control strategy is chosen such that the output voltage magnitude reference is aligned to the *d*-axis of the inverter reference frame, and the *q*-axis reference is set to zero.

$$v_{od}^* = v_n - n_q Q \qquad v_{oq}^* = 0 \quad ...(4)$$

The droop gains m_p and n_q are calculated using (5) for the given range of frequency and voltage magnitude

$$m_p = \frac{\omega_{max} - \omega_{min}}{P_{max}}, n_q = \frac{v_{odmax} - v_{odmin}}{Q_{max}} \quad ...(5)$$

As discussed earlier, to construct the complete model on a common reference frame, the reference frame of one of the inverters is taken as the common frame. To translate the variables from an individual inverter reference frame onto the common frame, we define an angle δ for each inverter, given in (6). It should be noted that δ represents the angle between an individual inverter reference frame and the common reference frame.

$$\delta = \int (\omega - \omega_{com}) \quad ...(6)$$

Now, to allow a simpler system representation, the *d* and *q* axis components of voltages and currents in the following equations are combined to form vectors as in (7).

$$v_{odq}^* = [v_{oq}^* v_{oq}^*]^T,\ i_{ldq} = [i_{ld} i_{lq}]^T$$

$$v_{odq} = \left[v_{od}\ v_{oq}\right]^T, i_{odq} = \left[i_{odq} i_{oq}\right]^T \quad ...(7)$$

By linearizing and rearranging the equations above, the small-signal power controller model can be written in a state-space form as in (8). The outputs of the power controller are the small-signal variation of output voltage reference and the frequency Δv_o*. Matrices of (8) are defined in (9). An additional input signal $\Delta\ \omega_{com}$, which is the frequency deviation of the common reference frame, is also included in the model. It facilitates the connection of an individual inverter model to the common reference frame. This aspect is explained in Section (II-B)

$$\begin{bmatrix}\Delta\dot{\delta}\\ \Delta\dot{P}\\ \Delta\dot{Q}\end{bmatrix} = A_P\begin{bmatrix}\Delta\delta\\ \Delta P\\ \Delta Q\end{bmatrix} + B_P\begin{bmatrix}\Delta i_{ldq}\\ \Delta v_{odq}\\ \Delta i_{odq}\end{bmatrix} + B_{P\omega com}[\Delta\omega_{com}]$$

$$\begin{bmatrix}\Delta\omega\\ \Delta V_{odq}^*\end{bmatrix} = \begin{bmatrix}C_{pw}\\ C_{pv}\end{bmatrix}\begin{bmatrix}\Delta\delta\\ \Delta P\\ \Delta Q\end{bmatrix} \quad ....(8)$$

$$A_P = \begin{bmatrix} 0 & -m_P & 0 \\ 0 & -\omega_c & 0 \\ 0 & 0 & -\omega_c \end{bmatrix} B_{P\omega com} = \begin{bmatrix} -1 \\ 0 \\ 0 \end{bmatrix} B_P$$

$$= \begin{bmatrix} 0 & 0 & 0 & 0 & 0 & 0 \\ 0 & 0 & \omega_c I_{od} & \omega_c I_{oq} & \omega_c V_{od} & \omega_c V_{oq} \\ 0 & 0 & \omega_c I_{oq} & -\omega_c I_{od} & -\omega_c V_{oq} & \omega_c V_{od} \end{bmatrix}$$

$$C_{p\omega} = [0 \quad -m_P \quad 0] C_{P\omega} = \begin{bmatrix} 0 & 0 & -n_q \\ 0 & 0 & 0 \end{bmatrix} \quad .....(9)$$

2.3 Voltage Controller

Output voltage control of the voltage controller is achieved with a standard PI controller. The corresponding state equations are

$$\frac{d\emptyset_d}{dt} = v_{od}^* - v_{od}, \frac{d\emptyset_q}{dt} = v_{oq}^* - v_{oq} \quad ....(10)$$

along with the algebraic equations

$$i_{ld}^* = F i_{od} - \omega_n C_f v_{oq} + K_{pv}(v_{od}^* - v_{od}) + K_{iv}\emptyset_d$$

$$i_{lq}^* = F_{ioq} + \omega_n C_f v_{od} + k_{PV}(v_{oq}^* - v_{oq}) + k_{iv}\emptyset_q \quad ....(11)$$

Equation (10) represent the linearized small-signal state-space form of the voltage controller. Here, the input to the subsystem is split into two terms: the reference input and the feedback inputs.

$$[\Delta\dot{\emptyset}_{dq}] = [0][\Delta\emptyset_{dq}] + B_{V1}[\Delta v_{odq}^*] + B_{V2}\begin{bmatrix} \Delta i_{ldq} \\ \Delta v_{odq} \\ \Delta i_{odq} \end{bmatrix} \quad ...(12)$$

In (12)

$$\Delta\emptyset_{dq} = [\Delta\emptyset_d \quad \Delta\emptyset_q]^T \quad ....(13)$$

$$B_{V1} = \begin{bmatrix} 1 & 0 \\ 0 & 1 \end{bmatrix}, B_{V2} = \begin{bmatrix} 0 & 0 & -1 & 0 & 0 & 0 \\ 0 & 0 & 0 & -1 & 0 & 0 \end{bmatrix} \quad ....(14)$$

$$[\Delta i_{ldq}] = C_v[\Delta\emptyset_{dq}] + D_{V1}[\Delta V_{odq}^*] + D_{V2}\begin{bmatrix} \Delta i_{ldq} \\ \Delta v_{odq} \\ \Delta i_{odq} \end{bmatrix} \quad ....(15)$$

$$C_V = \begin{bmatrix} k_{iv} & 0 \\ 0 & K_{iv} \end{bmatrix}, \qquad D_{v1} = \begin{bmatrix} K_{pv} & 0 \\ 0 & K_{pv} \end{bmatrix}$$

$$D_{V2} = \begin{bmatrix} 0 & 0 & -K_{pv} & -\omega_n C_f & F & 0 \\ 0 & 0 & \omega_n C_f & -K_{pv} & 0 & F \end{bmatrix} \quad ....(16)$$

2.4 Current Controller

Output filter inductor current control is achieved with a standard PI controller. The corresponding state equations are

$$\frac{d\gamma_d}{dt} = i_{ld}^* - i_{ld}, \frac{d\gamma_q}{dt} = i_{lq}^* - i_{lq} \quad ....(17)$$

along with the algebraic equations

$$v_{id}^* = -\omega_n L_f i_{lq} + K_{pc}(i_{ld}^* - i_{ld}) + K_{ic}\gamma_d \quad ....(18)$$

$$v_{iq}^* = \omega_n L_f i_{ld} + K_{pc}(i_{lq}^* - i_{lq}) + K_{ic}\gamma_q \quad ....(19)$$

Equation (17) represent the linearized small-signal state-space form of current controller

$$[\Delta\dot{\gamma}_{dq}] = [0][\Delta\gamma_{dq}] + B_{C1}[\Delta i_{ldq}^*] + B_{C2}\begin{bmatrix} \Delta i_{ldq} \\ \Delta v_{odq} \\ \Delta i_{odq} \end{bmatrix} \quad ....(20)$$

where

$$\Delta\gamma_{dq} = [\Delta\gamma_d \quad \Delta\gamma_q]^T \quad ....(21)$$

$$B_{C1} = \begin{bmatrix} 1 & 0 \\ 0 & 1 \end{bmatrix}, B_{C2} = \begin{bmatrix} -1 & 0 & 0 & 0 & 0 & 0 \\ 0 & -1 & 0 & 0 & 0 & 0 \end{bmatrix} \quad ....(22)$$

$$[\Delta v_{idq}^*] = C_C[\Delta\gamma_{dq}] + D_{C1}[\Delta i_{ldq}^*] + D_{C2}\begin{bmatrix} \Delta i_{ldq} \\ \Delta v_{odq} \\ \Delta i_{odq} \end{bmatrix} \quad ....(23)$$

$$C_C = \begin{bmatrix} K_{ic} & 0 \\ 0 & K_{ic} \end{bmatrix}, D_{C1} = \begin{bmatrix} K_{pc} & 0 \\ 0 & K_{pc} \end{bmatrix}$$

$$D_{C2} = \begin{bmatrix} -K_{pc} & -\omega_n L_f & 0 & 0 & 0 & 0 \\ \omega_n L_f & -K_{pc} & 0 & 0 & 0 & 0 \end{bmatrix} \quad ....(24)$$

2.5 Output LC Filter and Coupling Inductance

Output LC filter and the coupling inductance small-signal model can be represented with the following state equations by assuming that the inverter produces the demanded voltage *(vi=v*i)*:

$$\frac{di_{ld}}{dt} = \frac{-r_f}{L_f} i_d + \omega i_{lq} + \frac{1}{L_f} v_{id} - \frac{1}{L_f} v_{od} \quad \text{....(25)}$$

$$\frac{di_{lq}}{dt} = \frac{-r_f}{L_f} i_{lq} - \omega i_{ld} + \frac{1}{L_f} v_{iq} - \frac{1}{L_f} v_{oq} \quad \text{....(26)}$$

$$\frac{dv_{od}}{dt} = \omega v_{oq} + \frac{1}{C_f} i_{ld} - \frac{1}{C_f} i_{od} \quad \text{....(27)}$$

$$\frac{dv_{oq}}{dt} = -\omega v_{od} + \frac{1}{C_f} i_{lq} - \frac{1}{C_f} i_{oq} \quad \text{....(28)}$$

$$di_{od} = \frac{-r_c}{L_c} i_{od} + \omega i_{oq} + \frac{1}{L_c} v_{od} - \frac{1}{L_c} v_{bd} \quad \text{....(29)}$$

$$\frac{di_{oq}}{dt} = \frac{-r_c}{L_c} i_{oq} - \omega i_{od} + \frac{1}{L_c} v_{oq} - \frac{1}{L_c} v_{bq} \quad \text{....(30)}$$

The following equations represent the linearized small-signal state-space form of the LC filter and coupling inductance. Frequency ω_o is the system steady-state frequency at the given operating point:

$$\begin{bmatrix} \Delta i_{ldq} \\ \Delta v_{odq} \\ \Delta i_{odq} \end{bmatrix} = A_{LCL} \begin{bmatrix} \Delta i_{ldq} \\ \Delta i_{odq} \\ \Delta i_{odq} \end{bmatrix} + B_{LCL1}[\Delta v_{idq}] + B_{LCL2}[\Delta v_{bdq}] + B_{LCL3}[\Delta\omega] \quad \text{....(31)}$$

$$A_{LCL} = \begin{bmatrix} \frac{-rl_f}{L_f} & w_o & \frac{-1}{L_f} & 0 & 0 & 0 \\ -w_0 & \frac{-rl_f}{L_f} & 0 & \frac{-1}{L_f} & 0 & 0 \\ \frac{1}{c_f} & 0 & 0 & w_0 & \frac{-1}{c_f} & 0 \\ 0 & \frac{1}{c_f} & -w_0 & 0 & 0 & \frac{-1}{c_f} \\ 0 & 0 & \frac{1}{L_c} & 0 & \frac{-rl_c}{L_c} & w_0 \\ 0 & 0 & 0 & \frac{1}{L_c} & -w_0 & \frac{-rl_c}{L_c} \end{bmatrix}$$

$$B_{LCL2} = \begin{bmatrix} \frac{1}{L_f} & 0 \\ 0 & \frac{1}{L_f} \\ 0 & 0 \\ 0 & 0 \\ 0 & 0 \\ 0 & 0 \end{bmatrix} B_{LCL2} = \begin{bmatrix} 0 & 0 \\ 0 & 0 \\ 0 & 0 \\ 0 & 0 \\ \frac{-1}{L_c} & 0 \\ 0 & \frac{-1}{L_c} \end{bmatrix}$$

$$B_{LCL3} = [I_{lq} \quad -I_{ld} \quad V_{oq} \quad -V_{od} \quad I_{oq} \quad -I_{od}]^T \quad \text{...(32)}$$

2.6 Complete Model of an Individual Inverter

To connect an inverter to the whole system the output variables need to be converted to the common reference frame.

In this case the output variables of an inverter are the output currents represented as a vector Δi_{odq}. Using the transformation technique introduced, the small-signal output current Δ_{ioDQ} on the common reference frame can be obtained, as in (33).

$$[\Delta i_{oDQ} = [T][\Delta i_{odq}] + [T_c][\Delta\delta]] \quad \text{....(33)}$$

$$\text{where} T_s = \begin{bmatrix} \cos(\delta_\circ) & -\sin(\delta_\circ) \\ \sin(\delta_\circ) & \cos(\delta_\circ) \end{bmatrix}$$

$$T_c = \begin{bmatrix} -I_{od}\sin(\delta_\circ) - I_{oq}\cos(\delta_\circ) \\ I_{od}\cos(\delta_\circ) - I_{oq}\sin(\delta_\circ) \end{bmatrix} \quad \text{...(34)}$$

Similarly, the input signal to the inverter model is the bus voltage which is expressed on the common reference frame. The bus voltage can be converted to the individual inverter reference frame using reverse transformation, given by

$$[v_{bdq}] = [T_s^{-1}][\Delta v_{bDQ}] + [T_v^{-1}][\Delta\delta]$$

$$T_V^{-1} = \begin{bmatrix} -V_{bD}\sin(\delta_\circ) + \Delta V_{bQ}\cos(\delta_\circ) \\ -V_{bD}\cos(\delta_\circ) - V_{bQ}\sin(\delta_\circ) \end{bmatrix}$$

It is to be noted that the inverter whose reference frame is taken as the common reference frame has to provide its reference $\Delta\omega_{com}$ frequency to all the sub-modules of the model.

A complete state-space small-signal model of the inverter can be obtained by combining the state-space models of the power controller, voltage controller, current controller and output LC filter, There are totally 13 states, three inputs, and two outputs in each individual inverter model (except the inverter whose reference frame is the common reference frame, which has three outputs)

$$[\Delta\dot{x}_{invi}] = A_{INVi}[\Delta x_{invi}] + B_{INVi}[\Delta v_{bDQi}]B_{i\omega com} \quad \dots(35)$$

$$\begin{bmatrix}\Delta\omega_i \\ \Delta i_{oDQi}\end{bmatrix} = \begin{bmatrix}C_{INV\omega i} \\ C_{INVci}\end{bmatrix}[\Delta x_{invi}] \quad \dots(36)$$

where

$$\Delta x_{invi} = [\Delta\delta_i \;\; \Delta P_i \;\; \Delta Q_i \;\; \Delta\emptyset_{dqi} \;\; \Delta\gamma_{dqi} \;\; \Delta i_{ldqi} \;\; \Delta v_{odqi} \;\; \Delta i_{odqi}]^T$$

A. Combined Model of All the Inverters

In Section II-A5 the small-signal modeling of an individual DG inverter on a common reference frame was discussed. In a micro grid there can be several inverters acting as sources and connected remotely from each other. The modeling approach in this work is to form a sub-model of all the individual DG inverters and combine them with the network and individual load models.

Let us consider a system with *"s"* number of DG inverters where the reference frame of inverter number 1 is taken as the common reference frame. Then, from Section (II-A5), a combined small-signal model of all the inverter units together is obtained as shown in

$$[\Delta\dot{x}_{INV}] = A_{INV}[\Delta x_{INV}] + B_{INV}[\Delta v_{bDQ}] \quad \dots(37)$$

$$[\Delta i_{ODQ}] = C_{INVc}[\Delta x_{INV}] \quad \dots(38)$$

where

$$[\Delta x_{INV}] = [\Delta x_{inv1}\Delta x_{inv2} \dots . \Delta x_{inv\quad 8}]^T \quad \dots(39)$$

B. Network Model

An example network *n* of lines and m nodes with s inverters and *p* load points is shown in Figure 3. On a common reference frame the state equations of line current of ith line connected between nodes *j* and *k* are:

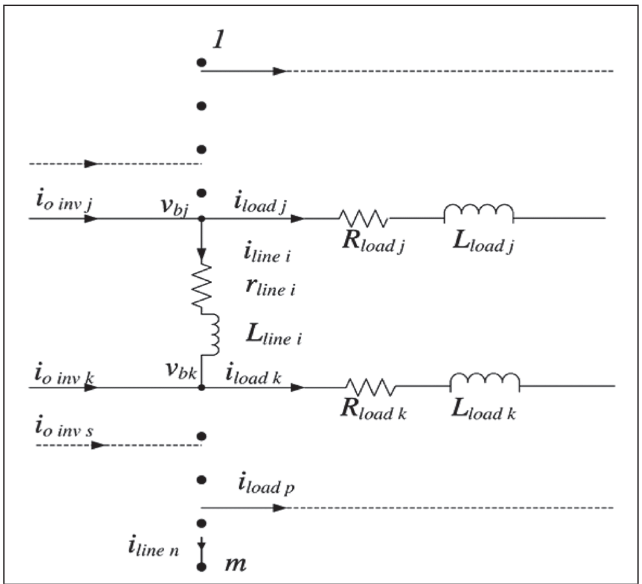

FIG. 3 NETWORK REPRESENTATION

$$\frac{di_{lineDi}}{dt} = \frac{-r_{linei}}{L_{linei}} i_{lineDi} + \omega i_{lineQi} + \frac{1}{L_{linei}} v_{bQj} - \frac{1}{Line_i} V_{bDk} \quad \dots(40)$$

$$\frac{di_{lineQi}}{dt} = \frac{-r_{linei}}{L_{linei}} i_{lineQi} - \omega i_{lineQi} + \frac{1}{L_{lineQj}} v_{bQj} \quad \frac{1}{L_{linei}} v_{bQk} \quad \dots(40)$$

Hence, the small-signal state-space model of a network with n lines is given by

$$[\Delta i_{lineDQ}] = A_{NET}[\Delta i_{lineDQ}] + B_{1NET}[\Delta v_{bDQ}] + B_{2NET\Delta\omega} \quad \dots(42)$$

In (42)

$$[\Delta i_{lineDQ}] = [\Delta i_{lineDQ1} \;\; \Delta i_{lineDQ2} \dots \Delta i_{lineDQn}]^T \quad \dots(43)$$

$$[\Delta v_{bDQ}] = [\Delta v_{bDQ1} \; \Delta v_{bDQ2} \dots . \Delta v_{bDQm}]^T \quad \dots(44)$$

$$\Delta = \Delta_{com} \quad \dots(45)$$

$$A_{NET}=\begin{bmatrix} A_{NET1} & 0 & \dots & 0 \\ 0 & A_{NET2} & \dots & 0 \\ \dots & \dots & \dots & \dots \\ 0 & 0 & \dots & A_{NET\ n} \end{bmatrix}_{2n\times 2n} \quad \text{....(46)}$$

$$B_{1NET}=\begin{bmatrix} B_{1NET1} \\ B_{1NET2} \\ \dots \\ \dots \\ B_{1NET\ n} \end{bmatrix}_{2n\times 2m}$$

$$B_{2NET}=\begin{bmatrix} B_{2NET1} \\ B_{2NET2} \\ \dots \\ \dots \\ B_{2NET\ n} \end{bmatrix}_{2n\times 1} \quad \text{...(47)}$$

where we get

$$A_{NETi}=\begin{bmatrix} \frac{-r_{linei}}{L_{linei}} & \omega_o \\ -\omega_o & \frac{-r_{linei}}{L_{linei}} \end{bmatrix} B_{2NETi}=\begin{bmatrix} I_{lineQi} \\ -I_{lineDi} \end{bmatrix}$$

$$B_{1NETi}=\begin{bmatrix} \dots & \frac{1}{L_{linei}} & 0 & \dots & \frac{-1}{L_{linei}} & 0 & \dots \\ \dots & 0 & \frac{1}{L_{linei}} & \dots & 0 & \frac{-1}{L_{linei}} & \dots \end{bmatrix}_{2\times(2m)} \quad \text{....(48)}$$

C. Load Model

Although, many types of load can exist in microgrids, a general RL load is considered in this paper. The state equations ofthe RL load connected at the ith nodes are:

$$\frac{di_{loadDi}}{dt}=\frac{-R_{loadi}}{L_{loadi}}i_{loadDi}+\omega i_{loadQi}+\frac{1}{L_{loadi}}v_{bDi} \quad \text{....(49)}$$

$$\frac{di_{loadQi}}{dt}=\frac{-R_{loadi}}{L_{loadi}}i_{loadQi}-\omega i_{loadDi}+\frac{1}{L_{loadi}}v_{bQi} \quad \text{....(50)}$$

Hence, for a network with load points the small-signal state space model of loads is given by

$$[\Delta i_{loadDQ}]=[\Delta i_{loadDQ}]+B_{1LOAD}[\Delta v_{bDQ}[\Delta v_{bDQ}] + B_{2LOAD}\Delta\omega \quad \text{....(51)}$$

In (51)

$$[\Delta i_{loadDQ}]=[\Delta i_{loadDQ1}\Delta i_{loadDQ2} \dots \Delta i_{loadDQ\ p}]^T \quad \text{....(52)}$$

$$A_{load}=\begin{bmatrix} A_{load1} & 0 & \dots & 0 \\ 0 & A_{load2} & \dots & 0 \\ \dots & \dots & \dots & \dots \\ 0 & 0 & \dots & A_{load\ p} \end{bmatrix}_{2p\times 2p} \quad \text{....(53)}$$

$$B_{2LOAD}=\begin{bmatrix} B_{2LOAD\ 1} \\ B_{2LOAD\ 2} \\ \dots \\ . \\ B_{2LOAD\ p} \end{bmatrix}_{2p\times(1)} \quad \text{....(54)}$$

Where

$$A_{loadi}=\begin{bmatrix} \frac{-R_{loadi}}{L_{loadi}} & \omega_o \\ -\omega_o & \frac{-R_{loadi}}{L_{loadi}} \end{bmatrix} B_{2LOADi}=\begin{bmatrix} I_{loadQi} \\ -I_{loadDi} \end{bmatrix}$$

$$B_{1LOADi}=\begin{bmatrix} \dots & \frac{1}{L_{loadi}} & 0 & \dots \\ \dots & 0 & \frac{1}{L_{loadi}} & \dots \end{bmatrix}_{2\times(2m)} \quad \text{...(55)}$$

D. Complete Microgrid Model

It can be seen in that the node voltages are treated as inputs to each subsystem. To ensure the node voltage is well defined (and that the numerical solution well conditioned) a virtual resistor is assumed between each node and ground. The resistance of virtual resistor T_N is chosen sufficiently large such that its introduction would have minimum influence on the dynamic stability of the system. Hence, the voltage of the node is given by

$$v_{bDi}=r_N(i_{oDi}-i_{loadDi}+i_{lineD\ i,j}) \quad \text{....(56)}$$

$$v_{bQi}=r_N(i_{oQi}-i_{loadQi}+i_{lineQ\ i,j}) \quad \text{....(57)}$$

In symbolic form, for a network with m nodes

$$[\Delta v_{bBQ}] = R_N\big(M_{INV}[\Delta i_{oDQ}] + M_{load}[\Delta i_{loadDQ}] + M_{NET}[\Delta i_{lineDQ}]\big) \quad \ldots(58)$$

In (58), matrix RN is of size *2mx2m,* whose diagonal elements are equal toT_N. The mapping matrix M_{INV} is of size *2mx 2m,* which maps the inverter connection points onto network nodes. For example, if ith inverter is connected at jth node, the element M_{INV} *(j,i)* will be 1 and all the other elements in that row will be 0. Similarly M_{load} are of size 2m x 2p maps load connection points onto the network nodes with -1. Matrix M_{NET} of size *2m x 2n* maps the connecting lines onto the network nodes. Here care

Root loci showing intera should be taken to put either +1 or -1 based on whether the given line current is entering or leaving the node. Now, the complete microgrid small-signal state-space model and hence the system state matrix can be obtained by using the individual subsystem models given in previous sections.

$$\begin{bmatrix} \Delta \dot{x}_{INV} \\ \Delta i_{lineDQ} \\ \Delta i_{loadDQ} \end{bmatrix} = A_{mg} \begin{bmatrix} \Delta x_{INV} \\ \Delta i_{lineDQ} \\ \Delta i_{loadDQ} \end{bmatrix} \quad \ldots(59)$$

The complete system state matrix A_{mg} is obtained and the small-signal flow among all the sub-modules is discussed in all the sections.

3.0 EIGENVALUE AND SENSITIVITY ANALYSIS

The eigen value concept of control theory has been extensively used to determine the stability of conventional power systems. Eigenvalues, termed modes, are the solution of the characteristic equation of a system's linearized state matrix [15]. This can be achieved with a sensitivity analysis conducted on the system state matrix. The sensitivity factor p_{ik} given by (60), is the measure of the association between the state variables and the modes and is equal to the sensitivity of the eigen value λ_i to the diagonal element *a kk* of the system state matrix. Sensitivity factors can be calculated using left and right eigenvectors

$$p_{ki} = \frac{\partial \lambda_i}{\partial a_{kk}} \quad \ldots.(60)$$

4.0 TEST SYSTEM MODEL

The test system shown in Figure 4 consist of three inverters of equal rating (10 kVA) with two load banks, one at each bus 1 and bus 3. These inverters are controlled to share the real and reactive powers over the lines1 and 2. System parameters are given in Table 1. Network is resistance dominated as is the case in low voltage distribution systems. DG1 and DG2 are located relatively close together compared to DG3. In this test system only resistive loads were used to verify the model. A resistive load of 5.8 kW (= 25Ω per phase) at bus 1 and 7.3 kW (20Ω per phase) at bus 2 is considered as an initial operating point.

In the test system analysed in this paper all the inverters are equally rated. Hence, the droop gains of all the inverters were chosen to be equal so that they equally share the fundamental power. The nominal frequency droop was 0.3% at the maximum real power output, whereas the nominal voltage droop was 2% at the maximum reactive power output. The choice of droop gains in such cases is further discussed in [16]. The objective of this paper is to investigate the stability of the system for the chosen values of droop gains. The model discussed in the previous section is general and it allows the users to investigate the system stability for any chosen combination of the system parameters.

In the design of the inverter output filter, the main criteria were to achieve attenuation by a factor of 100 in switching frequency ripple in the output voltage. This requires a resonant frequency of 10x less than the switching frequency, which is a common rule of thumb. The filter inductor value was chosen to have low ripple content in the inductor current and, when combined with the capacitor value, gives the required resonant frequency. A large coupling inductance results in a poor bus voltage regulation. Hence, in this application the coupling inductance was chosen to provide reasonable coupling impedance between the inverter output and the connection bus with a good bus voltage regulation. The proportional and integral gains of the voltage controller, shown in Table 1, were chosen using classical pole-zero and bode techniques to yield a bandwidth of 400 Hz for the voltage controller.

The current feed-forward gain was chosen to yield a low output impedance and hence improve the disturbance rejection of the inverter system.

The current controller was designed for 1.6-kHz bandwidth with good rejection of high-frequency disturbance. Although, the control was implemented in the discrete-time domain, the equivalent continuous domain gains are provided (in Table 1) for construction of the model.

TABLE 1

TEST SYSTEM PARAMETERS

Inverter parameters (10 kVA rating)			
Parameters	**Value**	**Parameters**	**Value**
f_s	8 KHz	m_p	9.4e-5
L_F	1.35 mH	n_q	1.3e-3
C_f	50	K_{pv}	0.05
r_f	0.1 Ω	K_{iv}	390
L_C	0.35 mH	K_{pc}	10.5
rL_C	0.03 Ω	K_{ic}	16e3
ω_C	31.41	F	0.75
Network and Local parameters (see Fig. 4)			

5.0 RESULTS

A. Small Signal Stability Results

A complete model of the test system was obtained using the procedure outlined in Section II. The steady-state operating point conditions were obtained from a MATLAB program simulation of the system. However, it is possible to use a more general load-flow solution as is often done in conventional power system modeling to obtain initial steady-state conditions [15]. The value chosen for virtual resistor (T_N) was 1000Ω.

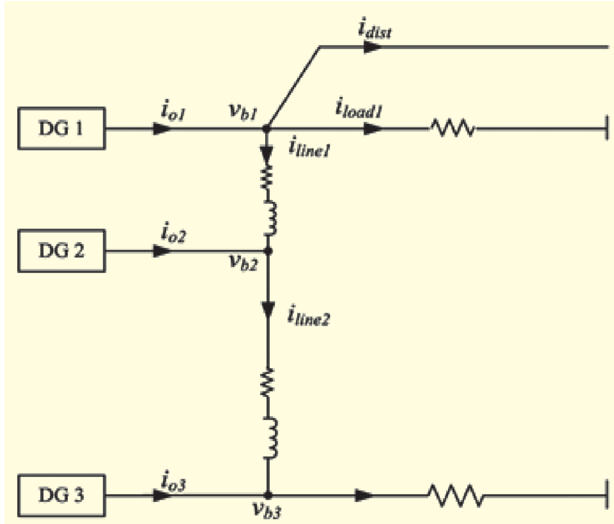

FIG. 4 TEST SYSTEM

TABLE 2

SENSITIVITY OF LOW FREQUENCY DOMINANT MODES

Sensitivity of		Sensitivity of	
state	**participation**	**state**	**participation**
P_1	0.15	P_1	0.12
Q_1	0.05	Q_1	0.06
P_2	0.3	P_3	0.32
Q_2	0.03	Q_3	0.03
δ_2	0.5	δ_3	0.57
Remaining states ≤0.005			

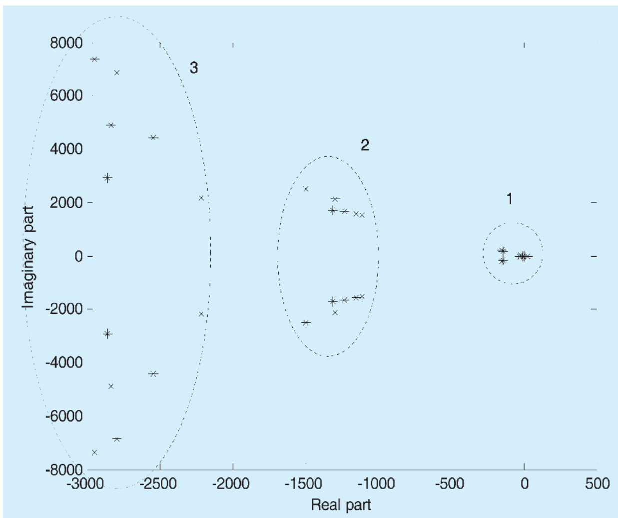

FIG. 5 EIGEN VALUE SPECTRUM OF THE SYSTEM INDICATING VARIOUS MODES.

Figure 5 shows the complete eigenvalues of the system. It can be seen that a large range of frequency components exist and that these fall in to three different clusters. Using (60), participation values of the power controller

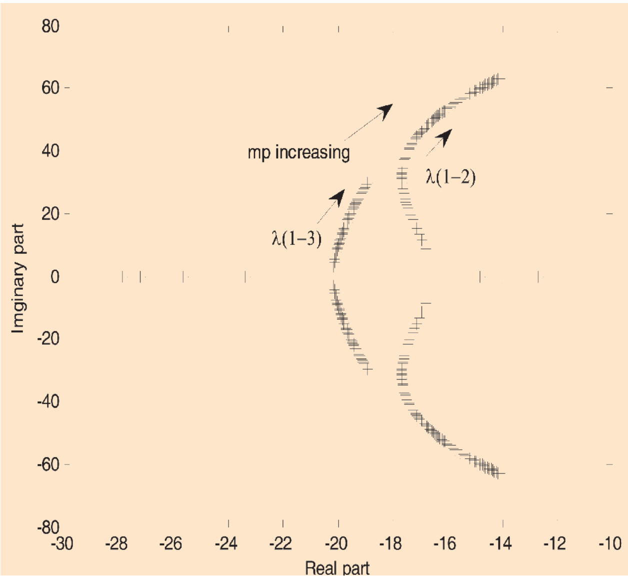

FIG. 6 TRACE OF LOW-FREQUENCY MODES AS A FUNCTION OF REAL POWER DROOP GAIN: 1.57E (0.05% DROOP) _ M _ 3.14E

Figure 6 shows the trajectory of the two-pairs of complex-conjugated dominant low frequency eigenvalues (part of cluster 1) as a function of the real power droop gain mp (the same value used for all the three inverters). The eigenvalues marked with λ1-2 are largely sensitive to the state variables of real power part of the power controllers of inverters 1 and 2, as given in Table 2. Similarly, eigen value marked as λ1-3 are highly sensitive to the state variables of real power part of the power controllers of inverters 1 and 3. It is therefore apparent that the modes λ1-2 and λ1-3 represent the dynamics of real power sharing of the DGs. However, these modes are also sensitive to the reactive power. This is a consequence of the coupling of real and reactive powers in the network due to the presence of highly resistive lines. Figure 6 shows that as is increased, modes λ1-2 and λ1-3 move towards unstable region making the system more oscillatory and eventually leading to instability. It is to be noted that large droop gain is necessary to improve the transient response of DGs, whereas a low-pass filter with low cut-off frequency is needed to achieve good attenuation of high frequency distortion components in the measured power and to avoid any interaction with inner current controllers.

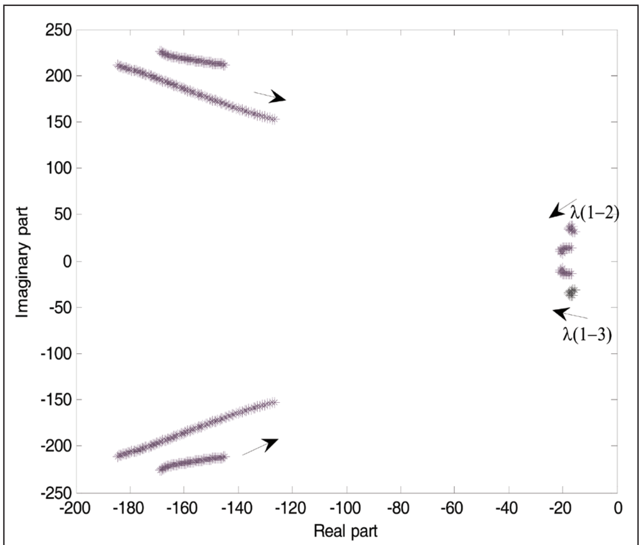

FIG. 7 TRACE OF LOW-FREQUENCY MODES AS FUNCTION OF REACTIVE POWER DROOP GAIN: 3.17E (0.5% DROOP) _ N _ 4.8E (8% DROOP)

Also, from Table 2 it can be observed that the dominant mode λ1-2 is highly sensitive to the states of the power controller of inverter 2. Hence, in this system, inverter 2 is the most critical element from the point of view of system stability. However, the low frequency dominant modes are less sensitive to the reactive power droop gain compared to the active power droop gain, as shown in Figure 7.

3.1 Transient Stability Results

In this section the eigenvalue results obtained from the model are used to verify the low frequency modes within the model. The disturbance was chosen to be a step change of 3.8-kW real power. A second set of tests was used to examine the low frequency modes under a severe step change in RL load connected at bus 1.

Figures 8–11 show the response of state variables P, and Q of all the three inverters obtained from the test model. Figure 8 shows the DG fundamental output power response for a 3.8-kW step change in load 1, for the test model.

In Figure 8 it can be seen that DG1, which is nearest to the changed load, took the major part of the transient whereas DG2 and DG3 have responded more slowly, depending on the effective impedance seen from the load point. Hence, during large changes in the load, closely located DGs may be overloaded and can be tripped out due to the limited overload capacity of the inverters.

Figure 9 shows the fundamental reactive power sharing. It can be seen that a considerable amount of reactive power was exchanged between the inverters even though the step was in the real power. This was because of the presence of significant resistance in the lines. This effect can be reduced by increasing the voltage magnitude droop but this will be at the expense of voltage quality.

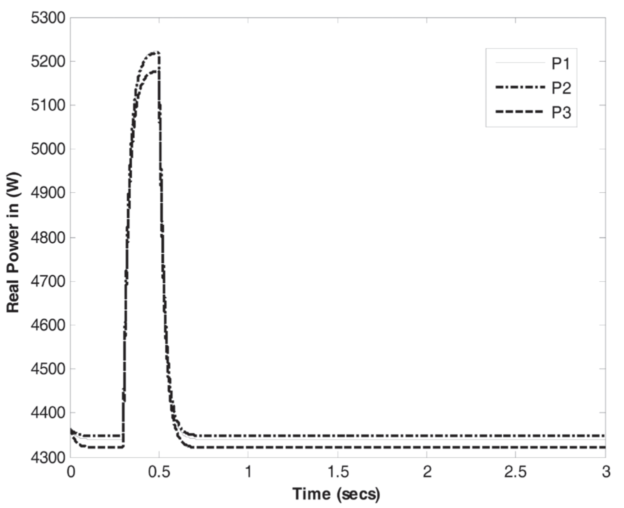

FIG. 8 ACTIVE POWER RESPONSE OF MICRO-SOURCES WITH 3.8 KW OF STEP CHANGE IN LOAD POWER AT BUS 1.

This is one of the major limitations of conventional droop control applied in low voltage grids [17], [18]. Again, it can be observed that the experimental results closely match the model results.

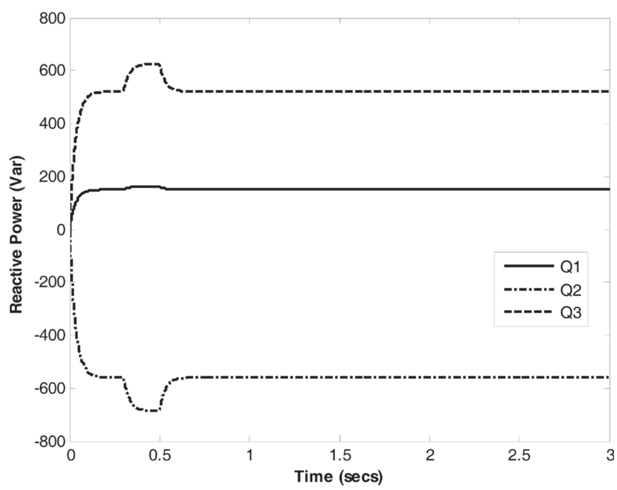

FIG. 9 REACTIVE POWER RESPONSE OF MICRO-SOURCES WITH 3.8 KW OF STEP CHANGE IN LOAD POWER AT BUS 1.

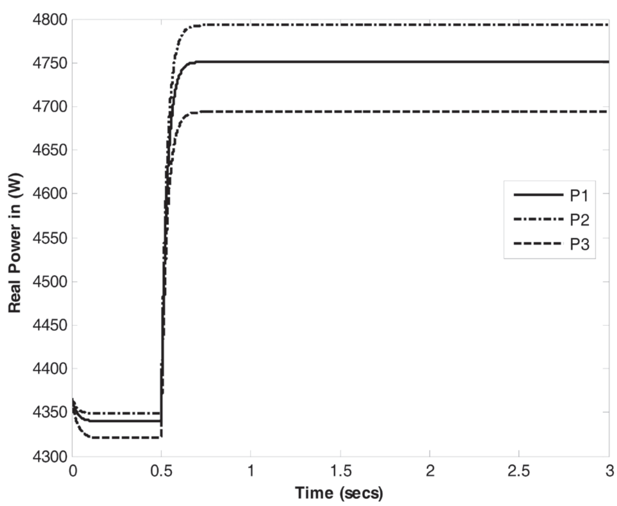

FIG. 10 ACTIVE POWER RESPONSE OF MICRO-SOURCES WITH 16.8 KW AND 12 KVAR RL LOAD STEP CHANGE AT BUS 1.

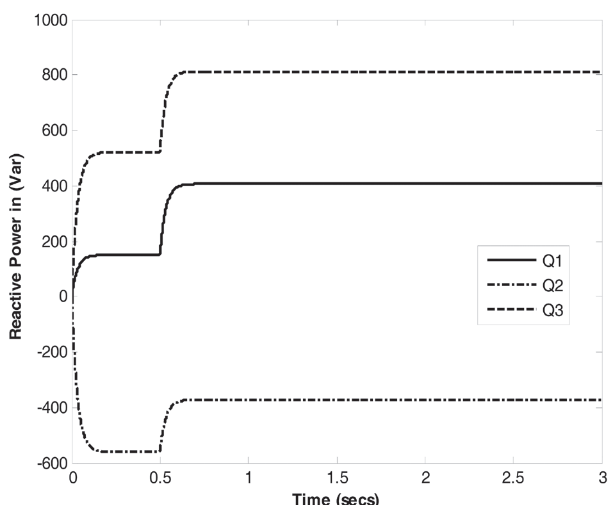

FIG. 11 REACTIVE POWER RESPONSE OF MICRO-SOURCES WITH 16.8 KW AND12 KVAR RL LOAD STEP CHANGE AT BUS 1.

To investigate the low frequency mode response under severe test load conditions, a test involving a step change of an RL load was conducted. In this test, there was initially no load connected to the system and then a load of 16.8 kW and 12 kVAR at bus1 was switched on. Figures 10 and 11 show the active and reactive power response of the inverters under such load transient. Also, it can be inferred that the reactive power sharing is rather poor in this case. However, this can be improved by increasing the reactive power droop gains but at the expense of poor bus voltage regulation.

6.0 CONCLUSION

In this paper, a small-signal state-space model of a microgrid is presented. The model includes inverter low frequency dynamics, high frequency dynamics, network dynamics, and load dynamics. All the sub-modules are individually modeled and are then combined on a common reference frame to obtain the complete model of the microgrid.

The model was analyzed in terms of the system eigen values and their sensitivity to different states. With the help of this analysis the relation between different modes and system parameters was established. It was observed that the dominant low-frequency modes are highly sensitive to the network configuration and the parameters of the power sharing controller of the micro sources. The high frequency modes are largely sensitive to the inverter inner loop controllers, network dynamics, and load dynamics.

Results obtained from the model were verified experimentally on a prototype microgrid. It was observed that the model successfully predicts the complete microgrid dynamics both in the low and high frequency range. Small signal modeling has had a long history of use in conventional power systems. The inverter models (and the inclusion of network dynamics) illustrated in this paper allow microgrids to be designed to achieve the stability margin required of reliable power systems.

REFERENCES

[1] R H Lasseter, "Microgrids," in Proc. Power Eng. Soc. Winter Meeting Jan 2002, vol.1, pp. 305-308.

[2] A Arulapalam , M Barnes, A Engler, A Goodwin, and N Jenkins, "Control of power electronic interfaces in distributed generation microgrids," IntJ. Electron., vol. 91,no. 9, pp. 503-523, Sep. 2004.

[3] R Lassetter, "Integration of Distributed Energy Resources: The CERTS Microgrid Concept," CERTRep., Apr. 2002.

[4] M S Illindla, P Piagi, H Zhang, G Venkataramanam, and R H Lasseter, "Hardware Development of a Laboratory-Scale Microgrid Phase 2:Operation and Control of a Two-Inverter Microgrid," Nat. Renewable Energy Rep.,Mar. 2004.

[5] Y Li, D M Vilathgamuwa, and P C Loh, "Design, analysis and real-time testing of A controller for multibus microgrid system,' IEEE Trans. Power Electron., vol. 19, no. 5, pp. 1195-1204, Sep. 2004.

[6] E A A Coelho, P Cortizo, and P F D Gracia, "Small signal stability for parallel-connected inverters in stand-alone ac supply systems," IEEE Trans. Ind. Appl., vol 38, no. 2, pp. 533-542, Mar./Apr. 2002.

[7] J M Guerrero, L G V Na, M Castilla, and J Miret,"A wireless controller to enhance Dynamic performance of parallel inverters in distributed generation systems,"IEEE Trans. Power Electron., vol. 19,no. 5, pp. 1205-1213, Sep. 2004.

[8] A L Dimeas and N D Hatziargyriou, "Operation of a multiagent system for microgrid Control," IEEE Trans. Power Syst., vol. 20, no. 3, pp. 1447-1455, Aug. 2005.

[9] M Prodanovic', T Green, and H Mansir," A survey of control methods for Parallel three-phase inverters connection,"Proc. Inst. Elect. Eng., no. 475, pp. 472-477, Sep. 2000.

[10] M C Chandorker, D M Divan, and A Rambabu, "Control of parallel connected inverters in stand-alone ac supply systems," IEEE Trans. Ind. Appl., vol. 29, no. 1, pp. 136-143, Jan./Feb. 1993.

[11] J M Undrill," Dynamic stability calculations for an arbitrary number of interconnected synchronous machines, "IEEE Trans. Power Apparat. Syst., vol PAS-87, no. 3, pp. 835-845, Mar. 1968.

[12] M N Marwali, J Jung, and A Keyhani," Control of distributed generation systems-part 11: load sharing control," IEEE Trans Power Electron., vol. 19, no. 6, pp. 1551-1561, Nov. 2004.

[13] M Prodanovic'," Power Quality and Control Aspects of Parrllel Connected Inverters in Distributed Generation," Ph. D. dissertation, Imperial College, Univ. London, Uk, 2004.

[14] M N Marwali, J Jung, and A Keyhani," Control of distributed generation systems-part1: voltages and current control," IEEE Trans Power Electron., vol. 19,no. 6, pp. 1541-1550, Nov. 2004.

[15] P Kundar, POWER SYSTEM STABILITY and CONTROL. New York: Mc Graw-Hill, 1994.

[16] C A Hernandez-Aramburo, T C Green, and N. Mugniot, "Fuel consumption minimization of a microgrid," IEEE Trans. Ind. Appl, vol. 41, no. 3, pp. 673-681, May/Jun. 2005.

[17] A Tuladhar, H Jin, T Unger, and K Mauch, "Control of parallel inverters in distributed ac power systems with considerations of line impedance effect," IEEE Trans. Ind. Appl, power vol. 36, no. 1, pp. 131-138, Jan./Feb. 2000.

[18] A Engler, "Applicability of droops in low voltage grids," Int. J. Distrib. Res., vol. 1, no. 1, pp. 3-15, Sep. 2004